The infuence of numerical diffusion on the solution of the radiative transfer equations

Jurgen Steinacker, Rémi Hackert, Adriane Steinacker, Aurore Bacmann

accepted for publication in **JQSRT**

THE INFLUENCE OF NUMERICAL DIFFUSION ON THE SOLUTION OF THE RADIATIVE TRANSFER EQUATIONS

Jürgen Steinacker[1], Remi Hackert[1], Adriane Steinacker[2], and Aurore Bacmann[1]

[1]Astrophysical Institute und University Observatory Jena, Schillergässchen 2-3, 07745 Jena, Germany

[2]NASA Ames Research Center 245-3, Moffett Field, CA 94035, USA

(*submitted 1 Februar 1999, Accepted 16 April 2001*)

Abstract — We investigate the explicit numerical solution strategies of multi-dimensional radiative transfer equations which are commonly used, e.g., to determine the radiation emerging from astrophysical objects surrounded by absorbing and scattering matter. For explicit grid solvers, we identify numerical diffusion as a severe source of error in first-order discretization schemes, underestimated in former work about radiative transfer. Using the simple example of a beam propagating through vacuum, we illustrate the influence of the diffusion on the solution and discuss various techniques to reduce it. In view of the large required storage for implicit solvers, we propose to use second-order explicit grid techniques to solve 3D radiative transfer problems.

1. INTRODUCTION

For many astrophysical applications, it is essential to know how the radiation is altered on its way from an object to the observer. Radiation will be scattered and absorbed by dust particles along the line of sight modifying the emerging spectrum of the enshrouded object. Hence, radiative transfer (RT) calculations are necessary to decompose original spectrum and changes due to external extinction, and are commonly used for analyzing young stellar objects, stars in late evolutionary stages, multiple stellar systems and active galactic nuclei.

Observations indicate that the distribution of matter around the objects deviates significantly from spherical symmetry (for young stellar objects see Sargent 1995[1], for active galactic nuclei see Lawrence 1987[2]). Flattened and toroidal structures interpreted as rotationally symmetric accretion disks, often accompanied by bipolar outflows point towards a more complex configuration of the gas and dust. Therefore, multi-dimensional radiative transfer is necessary to analyze all features of the observed spectra.

In the last decade, several methods have been proposed to treat axi-symmetric dust configurations with *2D continuum RT codes*, which we will summarize in the following..

The case of a cool, externally heated disk has been treated by Spagna & Leung 1987[3] applying a quasi-diffusion method. They proposed to solve the equation for rays travelling parallel through the medium in planes parallel to the figure axis. The ray equation was cast into a second-order combined equation and solved by finite differences on an equidistant 30×30 grid. A combined moment equation was used in diffusion approximation to determine the mean intensity, which is necessary to find the self-consistent temperature distribution with a Newton-Raphson iteration procedure.

Neglecting the influence of scattering, Dent 1988[4] calculated the temperature distribution of dust particles in a dense disk by tracing the radiation from the star and from the thermally emitting dust particles to a given point. The temperature distribution was iterated until it converged, the spatial structures was resolved by a 19×19 point grid on a mixed linear/logarithmic grid.

Efstathiou & Rowan-Robinson 1990[5] have presented results from a non-adaptive ray-tracer for flared disks assuming power-law densities in radius and azimuthal angle. In Efstathiou & Rowan-Robinson 1991[6], the dependency of the emergent spectrum of a protostar on model parameters has been discussed.

Two different density distributions around a single star have been investigated under the assumption of isotropic scattering by Collison & Fix 1991[7] using an iterative scheme.

The spectra of dust tori around active galactic nuclei have been analyzed by Pier & Krolik 1992[8] and Pier & Krolik 1993[9] with a 2D code based on a multi-dimensional Newton–Raphson technique, but neglecting scattering.

Sonnhalter et al. 1995[10] have applied a flux–limited approximation to derive spectra, temperatures, and intensities of several combinations of disk–halo distributions.

With an approximate 2D ray-tracer program, Menshchikov & Henning 1997[11] have analyzed flared disk configurations around young stellar objects. The same code was applied to active galactic nuclei by Manske et al. 1997[12]

There are only a few papers about grid-based codes for *3D continuum RT*. The three-dimensional effect becomes important in non-symmetric cases like binary systems, warped accretion disks, or multiple star formation. Yorke 1986[13] solved the frequency–dependent problem, but used a flux–limited approximation and omitted self-consistent

temperature iterations. Stenholm et al. 1991[14] treated the frequency–averaged problem for different axi-symmetric geometries. In both papers, grid methods are applied in conjunction with iterative methods to handle the large number of unknown intensities arising from the fact that stationary 3D continuum RT incorporates 3 variables in space, 2 in direction, and the frequency variable.

In all papers presenting grid-based 3D RT codes, numerical diffusion has not been considered and taken into account. The effect is well-known in the course of discretizating hyperbolic equations[19, and references therein].

In this paper, we will discuss the explicit grid-based algorithms to solve multi-dimensional radiative transfer equations and the arising errors due to numerical diffusion. We will not give a general outline of this type of numerical error, though, but rather concentrate on studying the effects in the case of RT equations. In Section 2, we analyze grid solvers based on an explicit first-order discretization and discuss the arising numerical diffusion using the simple example of a ray propagating through vacuum. Improvements by using optimized first-order grid solvers as well as schemes using higher-order discretizations are discussed in Section 3.

2. EXPLICITE FIRST-ORDER GRID SOLVERS FOR THE RADIATIVE TRANSFER EQUATION

2.1 The radiative transfer equation and the scattering integral problem

In this section, we will discuss the radiative transfer equation and simple solution strategies using explicit grid solvers. Generally, the equation for the specific monochromatic intensity $I_\nu(\vec{x},\vec{n})$ at the point $\vec{x}$ passing into the direction $\vec{n}$ given in spherical coordinates ϑ and φ is given by

$$\begin{aligned}\vec{n}\nabla I_\nu(\vec{x},\vec{n}) &= -\left[\sigma_\nu^{\rm abs}(\vec{x})+\sigma_\nu^{\rm sca}(\vec{x})\right] I_\nu(\vec{x},\vec{n})+\sigma_\nu^{\rm abs}(\vec{x})B_\nu[T(\vec{x})] \\ &\quad +\frac{\sigma_\nu^{\rm sca}(\vec{x})}{4\pi}\int\limits_\Omega I_\nu(\vec{x},\vec{n}')\ p_\nu(\vec{n},\vec{n}')d\Omega' \quad . \end{aligned} \tag{1}$$

For spherical dust particles as absorbing and scattering medium, we have

$$\sigma_\nu^{\rm abs,sca}(\vec{x}) = \pi a^2\ n(\vec{x})\ Q_\nu^{\rm abs,sca}, \tag{2}$$

where $Q_\nu^{\rm abs,sca}$ are the absorption and scattering coefficients, respectively, a is the dust particle radius, and $n(\vec{x})$ denotes the particle number density. $B_\nu[T(\vec{x})]$ represents the Planck function, $T(\vec{x})$ the temperature, and $p_\nu(\vec{n},\vec{n}')$ is the probability that radiation is scattered from the direction $\vec{n}$ into $\vec{n}'$.

Equation (1) is a 6D partial integro-differential equation and can be solved for the intensity if density and temperature of the dust distribution as well as the optical properties are known. Note that the dust temperature in turn depends on the radiation field, and that simultaneous solution of a local energy balance equation is necessary to determine intensity and temperature self-consistently.

The simple but robust source iteration strategy has been applied by Stenholm et al. 1991[12] for the solution of the RT equation with all three spatial coordinates. They discretize the simple first-order differential equation

$$\vec{n}\nabla I_\nu(\vec{x},\vec{n}) = -\left[\sigma_\nu^{\rm abs}(\vec{x})+\sigma_\nu^{\rm sca}(\vec{x})\right] I_\nu(\vec{x},\vec{n})+S_\nu(\vec{x},\vec{n}) \tag{3}$$

by an up-winding first-order finite differencing discretization scheme on an equidistant grid

$$\begin{aligned}\sin\vartheta\cos\varphi\frac{I_{i,j,k}^{\nu,\vartheta,\varphi}-I_{i-1,j,k}^{\nu,\vartheta,\varphi}}{\Delta x}+\sin\vartheta\sin\varphi\frac{I_{i,j,k}^{\nu,\vartheta,\varphi}-I_{i,j-1,k}^{\nu,\vartheta,\varphi}}{\Delta y}+\cos\vartheta\frac{I_{i,j,k}^{\nu,\vartheta,\varphi}-I_{i,j,k-1}^{\nu,\vartheta,\varphi}}{\Delta z} &= \\ -\left(\sigma_{i,j,k}^{abs;\nu}+\sigma_{i,j,k}^{sca;\nu}\right) I_{i,j,k}^{\nu,\vartheta,\varphi}+S_{i,j,k}^{\nu,\vartheta,\varphi}.\end{aligned} \tag{4}$$

for each ν, ϑ and φ. With this explicit scheme, the intensity $I_{i,j,k}^{\nu,\vartheta,\varphi}$ at each grid point (x_i,y_j,z_k) can be determined for each ν, ϑ and φ from the intensities $I_{i-1,j,k}^{\nu,\vartheta,\varphi}, I_{i,j-1,k}^{\nu,\vartheta,\varphi}, I_{i,j,k-1}^{\nu,\vartheta,\varphi}$ which already have been calculated or are given as boundary conditions.

To solve the scattering integral problem of the source term containing the unknown intensity,

$$S_\nu(\vec{x},\vec{n}) = \sigma_\nu^{\rm abs}(\vec{x})B_\nu[T(\vec{x})]+\frac{\sigma_\nu^{\rm sca}(\vec{x})}{4\pi}\int\limits_\Omega I_\nu(\vec{x},\vec{n}')\ p_\nu(\vec{n},\vec{n}')d\Omega' \ , \tag{5}$$

Stenholm et al. 1991[14] applied a fix-point method, the well-known "Λ-iteration". Starting with an initial source term, (4) is solved for a new intensity and using (5) a new source

term is calculated. This procedure is iterated until convergence is achieved and the convergence rate can be accelerated by methods like the one proposed in Ng 1974[15]. The advantage is that the explicit scheme allows fast solution of (4), saving computer time for the iterations to determine the scattering integral and the self-consistent temperature.

2.2 Discretization error on the spatial and direction grid

For all applications of discretized schemes, the control of numerical errors is an imperative part of the solution analysis. The error arising from the discretization of the propagation direction (ϑ, φ) will not be discussed in this paper. We just emphasize that the multivariant discretization used in Stenholm et al. 1991[14] is not optimal for integrations on the unit sphere and we refer to Steinacker et al. 1996[16] for an optimized node distribution and corresponding weights.

We also do not discuss moment corrections often used in discretized RT problems. The influence of discretizing a transport equation with a limited number of propagation directions, e.g., has been investigated by Lathrop (1968)[20]. This "ray effect" results in extra moments in the derived moment equations, and the author derives a method adding an anisotropic source term to correct for ray effects.

The spatial discretization error of the explicit scheme can be illustrated by analyzing the simplified 1D RT equation

$$\frac{dI}{dx} = -\sigma I \tag{6}$$

with the solution $I = I_0 \exp\left[-\int \sigma dx\right]$. Applying the first-order finite differences scheme yields $I_i \ (1 + \sigma_i \Delta x) = I_{i-1}$ and for $|\sigma_i \Delta x| \ll 1$, we have $I_i \approx e^{\sigma_i \Delta x} I_{i-1}$ in approximate agreement with the analytic solution, since $x_i = x_{i-1} + \Delta x$.

The necessary condition $|\sigma_i \Delta x| \ll 1$ is absolutely crucial for applications with steep spatial gradients. In the inner parts of accretion disks, e.g., the density dependency on the distance to the central object is typically characterized by a power-law, so that an equidistant grid with numbers of grid points < 100 cannot be expected to fulfill this condition. Improvements can be achieved by using adaptive regular grids, which do minimize the local optical depth $\tau_i = \int_{x_{i-1}}^{x_i} \sigma(s) ds$ or by using Runge-Kutta integral methods.

2.3 Numerical diffusion of explicit discretization schemes

While the spatial discretization error depends on the used density distribution and the properties of the enshrouding medium, another purely numerical error occurs in connection with the used explicit first-order scheme. The neglected second-order discretization terms cause the well-known *numerical diffusion* error, called like this due to the interpretation of second-order terms in physical problems as diffusion. To illustrate its effect on the solution and its independency on the physical conditions, we assume the simple test

case of a beam of radiation propagating through vacuum. This type of equation is equal to that of an advection equation being used in hydrodynamics. Hence, $\sigma_\nu^{abs,sca}$ and B_ν are zero and restricting to propagation in the x-y-plane, (4) reads

$$\cos\varphi \frac{I_{i,j}^{\nu,\varphi} - I_{i-1,j}^{\nu,\varphi}}{\Delta x} + \sin\varphi \frac{I_{i,j}^{\nu,\varphi} - I_{i,j-1}^{\nu,\varphi}}{\Delta y} = 0 \tag{7}$$

or choosing a symmetric grid $\Delta x = \Delta y$

$$I_{i,j} = \frac{\cos\varphi I_{i-1,j} + \sin\varphi I_{i,j-1}}{\cos\varphi + \sin\varphi}. \tag{8}$$

The beam is achieved by assuming the boundary conditions $I_{i,j} = 0$ except $I_{0,0} = I_{0,1} = I_{1,0} = I_0$. Intuitively, we expect the beam to propagate through the grid undisturbed.

Fig. 1 shows the radiation field after applying (8) for 100 grid points and $\varphi = 45°$ as a contour plot. Obviously, the beam peak intensity decreases during propagation as illustrated in Fig. 2, where we have plotted this decrease expressed as a percentage. We find that the beam height drops down to 10% of the original value at the end of the grid.

While Fig. 1 seems to indicate that the beam stays collimated after a slight divergence in the beginning, Fig. 3 illustrates the widening of the beam half width up to 10 grid cells at the grid border.

For the case of $\varphi = 45°$, it is easy to show that the integral beam intensity is conserved, but redistributed under the process of numerical diffusion. Using the binomial coefficients $\binom{n}{k}$, the intensity at the point (x_i, y_j) is

$$I_{i,j} = 2^{4-i-j} \binom{i+j-4}{j-2} I_0. \tag{9}$$

For cuts perpendicular to the beam propagation direction at distance $n\Delta x/\sqrt{2}$ from the origin, the integral along $\vec{s} \perp (\cos\varphi, \sin\varphi)$ can be approximated by

$$\int_{-\infty}^{+\infty} I ds \approx \sum_{k=0}^{n} I_{k,n-k} \sqrt{2}\Delta x = \sqrt{2}\Delta x \; 2^{-n} I_0 \sum_{k=0}^{n} \binom{n}{k} = \sqrt{2}\Delta x \; I_0. \tag{10}$$

Hence, the area below the intensity curve does not change with n. The intensity of the beam is just redistributed into a descending Gaussian beam as it can be seen also from Fig. 4, where we have plotted the intensity along an ordinate perpendicular to the beam.

The numerical diffusion depends on φ. For $\varphi = 0°$ and $\varphi = 90°$, $I_{i,j} = I_{i-1,j}$ and $I_{i,j} = I_{i,j-1}$, respectively, and the effect vanishes. Since the problem is chosen to be symmetric in x and y, maximal diffusion occurs at $\varphi = 45°$.

The effect of diffusion is even more severe in the 3D case, as the intensity can be spread in one more direction. We will quantify the differences between 2D and 3D while discussing possible ways to reduce the diffusion.

Before that, we will try to answer the question what effect the numerical diffusion has on the results of RT calculations. For non-vanishing dust density, the beam will decollimate due to scattering and re-emission of the radiation. Convolving this with the numerical diffusion will increase the smoothing of sharp features. Hence, it is understandable that little attention was paid to this effect as it is hard to distinguish from the

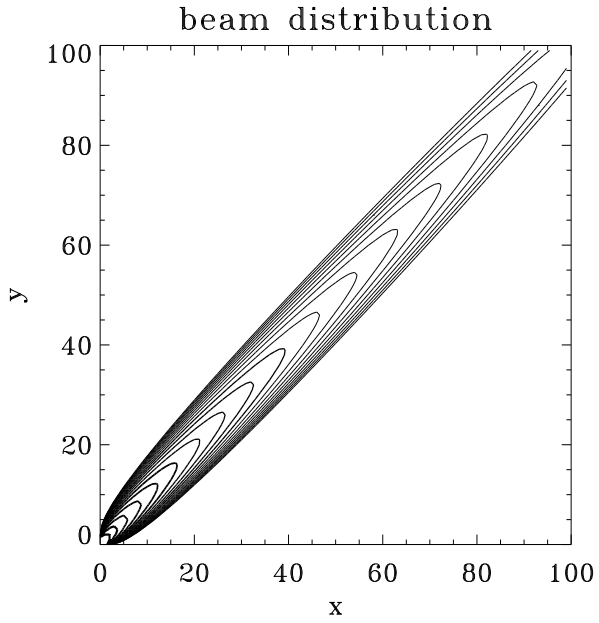

Figure 1: 2D-intensity distribution for a beam propagating in vacuum. The contour lines indicate that the beam diverges due to the influence of the numerical diffusion.

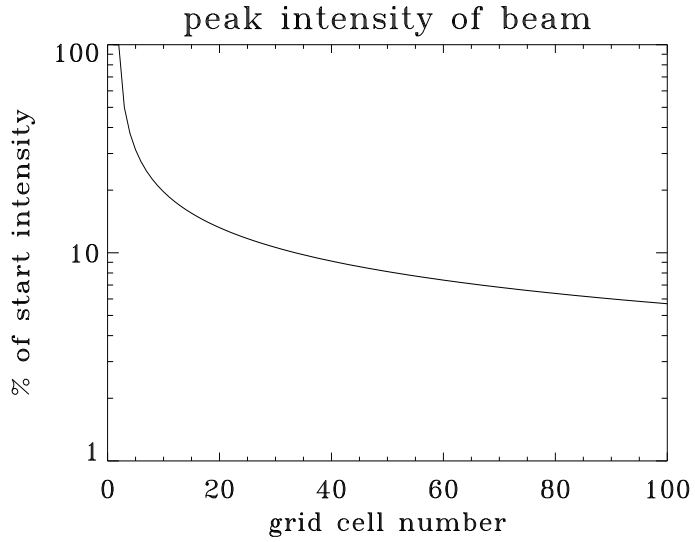

Figure 2: Beam peak height as function of grid cell number along the line of sight. The numerical diffusion reduces the height by a factor of 6.5 within the first 15 grid points.

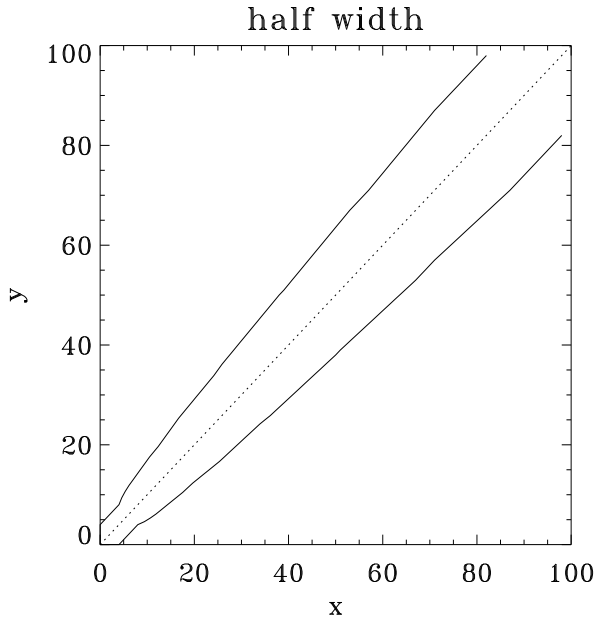

Figure 3: Half width of the beam. At the outer boundary, the width has increased by a factor of 10.

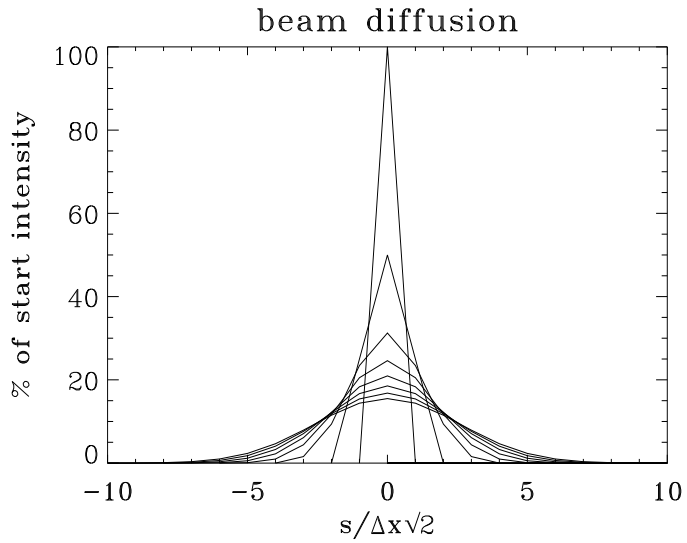

Figure 4: Radiation field as a function of the coordinate s perpendicular to the beam direction which is normalized to a grid cell diagonal. The start intensity distribution alters under the effect of diffusion to a descending Gauss function. The curves show $I(s)$ with $s/\Delta x\sqrt{2}\ \epsilon\ [0, 7]$.

smoothing due to the dust. Fig. 5 shows an illustrative intensity pattern in an ordinate perpendicular to the line of sight. The numerical diffusion smoothes all sharp features, and after 50 grid points, the oscillations can hardly be identified (dash-dotted line). At the outer border of the grid, any detailed spatial information is lost (dashed line) and only the overall shape of the pattern is conserved.

The simplest way to avoid the diffusion is to increase the resolution of the grid, if the physical application allows for this.

In Fig. 6, the peak intensity at three locations in the grid is plotted as a function of the grid refinement step (factor 2 refinement) of the original 10×10 grid for the case of maximal diffusion $\varphi = 45°$. Dots, crosses, and diamonds give the values at points directly after the beam injection point, in the middle, and at the end of the grid, respectively. Obviously, 180×180 grid points are required to reduce the decrease of the beam peak size to 80%.

Clearly, the beam stays collimated at high resolutions, and an appropriate resolution can be chosen from this figure that fits the error requirements of a special application. This also reveals the purely numerical nature of the diffusion effect.

The corresponding figure for 3D RT (Fig. 7) reveals the effect of numerical diffusion even better. Here, a grid of about $400 \times 400 \times 400$ is necessary to avoid beam peak decrease below 80%.

For hyperbolic equations like this simple advection equation, several methods have been proposed to analyze and handle errors due to numerical diffusion (e.g. Vichnevetsky & Bowles 1995[19]), including Fourier analysis and filtering. For 3D RT problems, however, those algorithms are much too time-consuming as they are 6 dimensional while hyperbolic problems e.g. in time-dependent hydrodynamics are 4 dimensional. Hence, we are looking for a less time-consuming and robust algorithm, which decreases the effect of numerical diffusion.

3. IMPROVED EXPLICIT SOLVERS TO AVOID NUMERICAL DIFFUSION

3.1 Improved first-order schemes

Using more general first-order explicit schemes, it should be possible to come up with a discretization minimizing the numerical diffusion. Approximating e.g. the derivative in x-direction as

$$\left.\frac{\partial I}{\partial x}\right|_{(x_i,y_j)} = \frac{[s_1 I_{i,j} + (1-s_1)\, I_{i,j-1}] - [s_1 I_{i-1,j} + (1-s_1)\, I_{i-1,j-1}]}{\Delta x} \tag{11}$$

we can choose the free parameter s_1 (for details see Koren 1991[17]) so that the diffusion from the neglected second-order terms is minimal. It turns out that only the mixed second-order term $\partial^2 I / \partial x \partial y$ can be forced to vanish. Hence, it cannot be expected to fix the problem of numerical diffusion with an optimized explicit first-order discretization

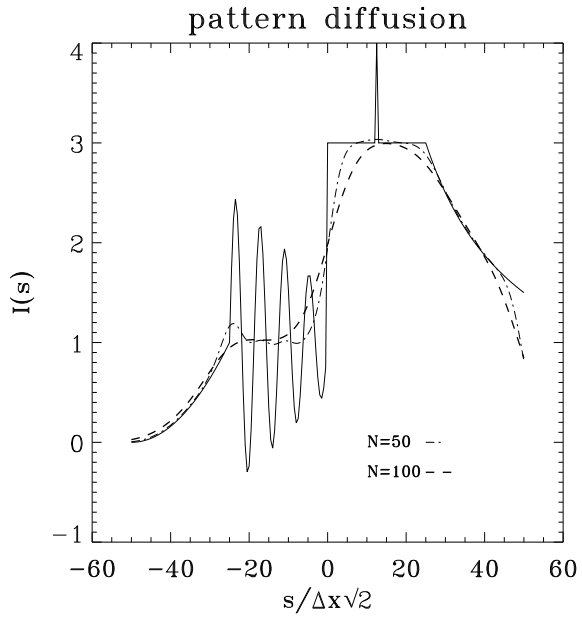

Figure 5: Smoothing of an illustrative intensity pattern due to numerical diffusion in the 2D case (diagonal propagation). The solid line represents the original pattern, the dash-dotted line shows the pattern seen in the middle of the grid, the dashed line give the pattern at the grid border.

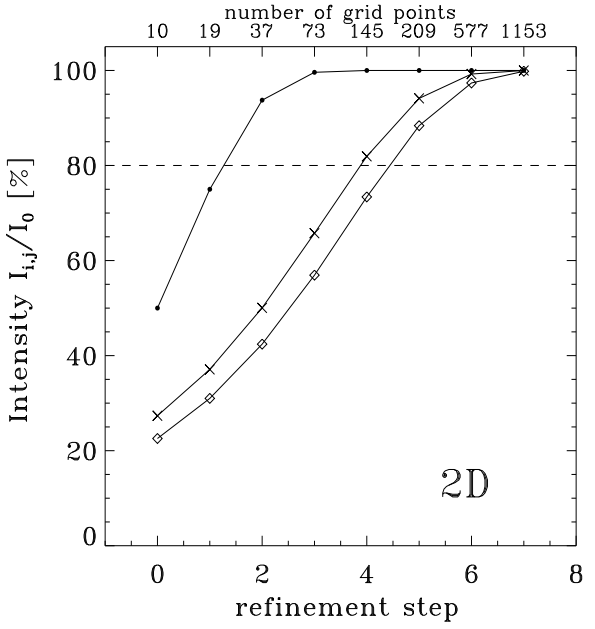

Figure 6: 2D-diagonal beam intensity as a function of the grid refinement for a point closely after beam origin (dots), in the middle of the grid (crosses), and at the border of the grid (diamonds). The top axis gives the number of grid points in one direction, the dashed line represents an illustrative level of error acceptance.

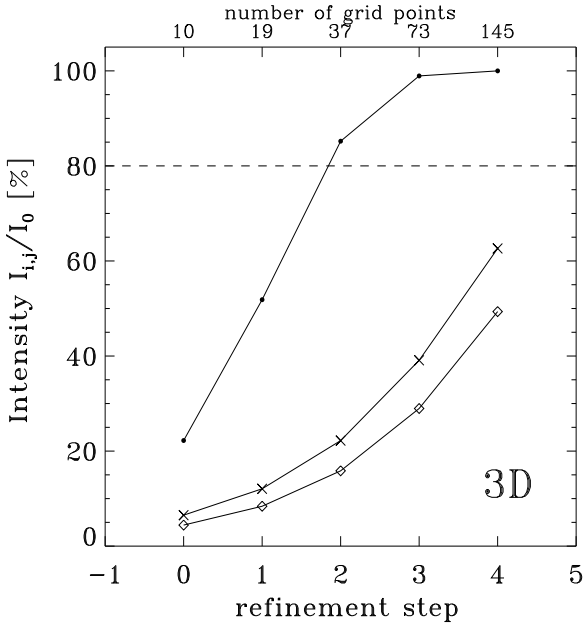

Figure 7: 2D-diagonal beam intensity as a function of the grid refinement for a point closely after beam origin (dots), in the middle of the grid (crosses), and at the border of the grid (diamonds). The top axis give the number of grid points in one direction, the dashed line represents an illustrative level of error acceptance.

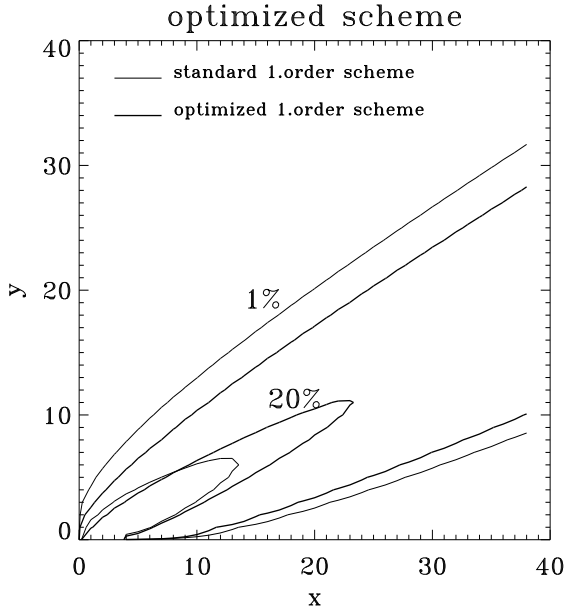

Figure 8: Comparison of the intensity contours at 1% and 20% for the standard (thin line) and optimized (thick line) first-order discretization scheme. The beam propagating with an angle of 25° to the x-axis is better confined in the optimized calculation, but the error due to numerical diffusion is still prominent.

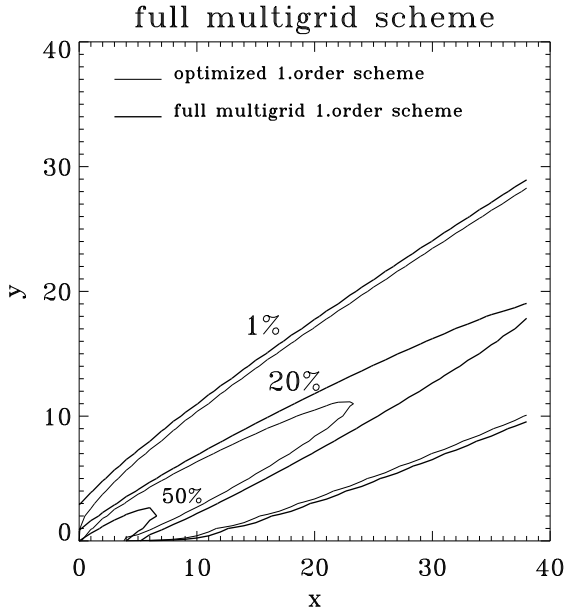

Figure 9: Comparison of the intensity contours at 1% and 20% for the optimized first-order discretization (thin line) and a full multigrid scheme (thick line). The beam propagating with an angle of 25° to the x-axis is better confined for the inner parts of the beam in the multigrid calculation. The 50%-level is also shown for the multigrid scheme.

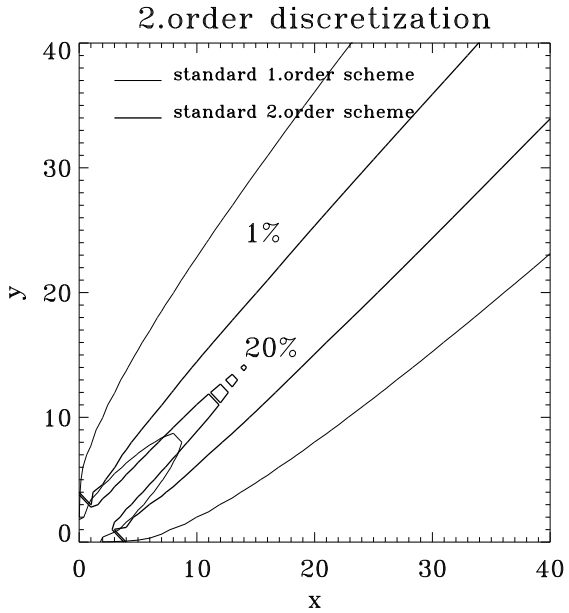

Figure 10: Comparison of the intensity contours at 1% and 20% for the standard first-order (thin line) and second-order discretization scheme (thick line). The diagonally propagating beam stays confined in the second-order calculation, but still a smoothing due to higher-order terms is present. The oscillation of the 20% beam of the standard 2.order scheme is caused by plotting the iso-contours for a radiation field known only on a finite grid and is therefore not real.

scheme in the general case. This is especially valid for the RT problem, as can be seen in our 2D-vacuum test case. Applying the optimized value of s_1 to (11) yields

$$I_{i,j} = \frac{\left[\cos^2\varphi I_{i-1,j} + \cos\varphi \sin\varphi I_{i-1,j-1} + \sin^2\varphi I_{i,j-1}\right]}{1 + \cos\varphi \sin\varphi} . \tag{12}$$

Fig. 8 shows the resulting differences between the beam confinement for $\varphi = 25°$ in the 2D-case. Although the 1% and 20% contours indicate that the beam is better confined in the optimized calculation, the effect of numerical diffusion is still prominent.

A further improvement to the simple first-order discretization solution can be the application of multigrid methods. We used a self-developed full multigrid cycle program to the vacuum test problem and used a black white Gauss-Seidel smoother (see e.g. Hackbusch 1993[18]). The cycles were repeated until convergence was achieved with 2–3 smoothing steps and second-order restriction and interpolation was used for the inter-grid communication. The calculated radiation distribution is plotted in Fig. 9 for the optimized first-order scheme and the full multigrid scheme. While the beam has even broadened slightly at the 1%-contour level, it shows better collimation in the inner parts in the multigrid calculation. As the multigrid algorithm uses the information of finer grids - where the numerical diffusion is smaller - to improve the correctness of the solution, it is evident that the multigrid calculation leads to better results. The diffusion, however, does not vanish, and in view of the efforts to run a multigrid algorithm, we conclude that first-order multigrid methods do not solve the problem of numerical diffusion in RT calculations.

3.2 Explicit higher-order schemes

Higher-order discretization schemes require more boundary informations and will use more computer time. Nevertheless, an explicit formulation is possible and applicable to the RT equation. Approximating the derivative by the derivative of a parabola through the points $(x_k, y_l),\ k = i, i-1, i-2,\ l = j, j-1, j-2$, we have

$$\left.\frac{\partial I}{\partial x}\right|_{x_i, y_j} = \frac{\Delta x \left(I_{i-2} - 4I_{i-1} + 3I_i\right)}{x_{i-2}^2 - 2x_{i-1}^2 + x_i^2} \tag{13}$$

and find for the explicit scheme

$$I_{i,j} = \frac{A}{3\left(A+B\right)}\left(4I_{i-1,j} - I_{i-2,j}\right) + \frac{B}{3\left(A+B\right)}\left(4I_{i,j-1} - I_{i,j-2}\right) \tag{14}$$

with

$$A \equiv \frac{\cos\varphi}{x_{i-2}^2 - 2x_{i-1}^2 + x_i^2} \tag{15}$$

$$B \equiv \frac{\sin\varphi}{y_{j-2}^2 - 2y_{j-1}^2 + y_j^2} \tag{16}$$

In Fig. 10, the resulting beam patterns of this scheme is compared to the standard first-order scheme. The beam is much better collimated in the second-order case.

Although third-order discretizations can be expected to have even lower numerical diffusion errors, the computer time to calculate each derivative is 7 times larger than in the second-order case. Hence, for most multi-dimensional radiative transfer applications, we recommend to use the explicit second-order discretization which shows little numerical diffusion, does not need extended computer storage like the implicit schemes, and is still fast enough to perform 3D radiative transfer calculations.

Acknowledgements–We thank Th. Henning for helpful comments. This work was supported by the Max Planck Society (J.S. and R.H.) and the German Research Foundation (A.S. STE 845/1-1).

REFERENCES

1. Sargent, A.I., in: *Disks and Outflows around Young Stars*, S.V.W. Beckwith, A. Natta, J. Staude (Eds.), Springer, Berlin, Heidelberg (1995)
2. Lawrence, A., PASP 99, 309 (1987)
3. Spagna, G.F., Leung, C.M., JQSRT 37, 565 (1987)
4. Dent, W.R.F., ApJ 325, 252 (1988)
5. Efstathiou, A., Rowan-Robinson, M., MNRAS 245, 275 (1990)
6. Efstathiou, A., Rowan-Robinson, M., MNRAS 252, 528 (1991)
7. Collison, A.F., Fix, J.D., ApJ 368, 545 (1991)
8. Pier, E.A., Krolik, J.H., ApJ 401, 99 (1992)
9. Pier, E.A., Krolik, J.H., ApJ 418, 673 (1993)
10. Sonnhalter, C., Preibisch, Th., Yorke, H.W., A&A 299, 545 (1995)
11. Menshchikov, A., Henning, Th., A&A 318, 874 (1997)
12. Manske, V., Henning, Th., Menshchikov, A., A&A, 331, 52 (1998)
13. Yorke, H., W., in: *Astrophysical Radiation Hydrodynamics*, K.–H. Winkler, M.L. Norman (Eds.) (Reidel, Dordrecht), 141 (1986)
14. Stenholm, L.G., Störzer, H., Wehrse, R., JQSRT 45, 1, 47 (1991)
15. Ng, K.-C., JCP, 61, 7, 2680 (1974)
16. Steinacker, J., Thamm, E., Maier, U., JQSRT 56, 1, 97 (1996)
17. Koren, B., in: *Defect Correction for Multidimensional Euler Flows* (Birkhauser, Basel), Intern. Series of Numerical Math. 98 (1991)
18. Hackbusch, W., in: *Iterative Lösungen großer schwachbesetzter Gleichungssysteme* (Teubner, Stuttgart) (1993)
19. Vichnevetsky, R., Bowles, J.B., in: *Fourier Analysis of Numerical Approximations of Hyperbolic Equations* (SIAM 5, Philadelphia) (1995)
20. Lathrop, K.D., Nucl. Sci. Eng. 32, 357 (1968)